Modeling the Effect of Soluble Group I Fission Isotope (Rb, Cs) Chlorides on the Phase Behavior of Multi-Component Molten Salt Reactor Chloride Fuels

Woei Jer Ng [a], Ho Jin Ryu [a,b*]
[a]*Department of Nuclear and Quantum Engineering, KAIST, Daejeon, Yuseong-gu 34141, Republic of Korea*
[b] *Department of Materials Science and Engineering, KAIST, Daejeon, Yuseong-gu 34141, Republic of Korea*
[*]*Corresponding author: hojinryu@kaist.ac.kr*

1. Introduction

Molten Salt Reactors (MSR) are a subset of nuclear fission reactors proposed as early as the 1950s. The designation of MSRs as one of the six Generation IV reactor concepts has largely rekindled interest in MSR technology. This renewed interest can be ascribed to the wide range of potential advantages associated with MSR operation, such as reduced operation costs, higher thermal efficiency, homogeneous fuel composition [1], and low radioactive waste production [2]. More importantly, the inherent safety of MSR reactors is further augmented by its strong negative temperature coefficient and its operation at atmospheric pressure (which eliminates radioactive release due to the presence of large pressure gradients) [3].

The molten salts employed in MSRs are commonly categorized based on their anions, namely fluorides and chlorides. While studies on fluoride salts have historically garnered more attention, chloride salts may offer several key advantages over their fluoride counterparts, such as lower melting temperatures, more diverse methods for fuel-salt separation, improved solubility for actinides [4], and lower corrosivity [5]. Moreover, in terms of neutronics, the higher Z value of chlorine is more beneficial towards preserving the fast neutron spectrum during reactor operation.

In 2008, Benes and Konings published their work on the comprehensive thermodynamic modeling of the $NaCl$-$MgCl_2$-UCl_3-$PuCl_3$ system [6]. Their work is the first known attempt at predicting the phase composition of high-order multi-component MSR chloride fuel systems using CALPHAD simulations. While their work provides salient insight towards the optimization of the initial composition of MSR fuel salt systems, the nature of nuclear fission dictates a continuous change to the fuel composition upon operation. Hence, the transient behavior of the fuel composition due to the formation of fission isotopes opens up an avenue for further investigation.

In this work, we attempt to probe the effects of Group I fission products (Rb, Cs) on the phase behavior of the proposed $NaCl$-$MgCl_2$-UCl_3-$PuCl_3$ system using similar CALPHAD simulation techniques.

2. Methodology

The thermochemical data of all chloride salts (end-members) and a majority of the intermediate compounds used in this simulation were obtained from the ORNL Molten Salt Thermodynamic Database (MSTDB) [7]. In the case whereby the thermochemical data of intermediate compounds are unavailable, C_p was calculated from the molar-weighted sums of its constituent salts, whereas the values of H_{298K} and S_{298K} were estimated. All the estimated thermodynamic parameters used in this simulation are provided in Table 1.

Binary phase diagrams between all combinations of the constituent end-members (except $RbCl$ - $CsCl$) were reconstructed using FactSage 8.1. The excess Gibbs' free energy of non-ideal mixing (G^{ex}) solutions was modeled using the Two-Lattice Modified Quasichemical Model (MQM), whereas that for solid solutions was modeled by applying the Redlich-Kister equation in the classical "One-lattice Polynomial Model" (QKTO). The vast majority of the

Table 1. *Estimated thermochemical data for intermediate compounds in $RbCl$-UCl_3 and $CsCl$-UCl_3 binary phase diagrams.*

	H_{298K} (kJ)	S_{298K} (J/K)	$C_p(T)$ $(J/kg \cdot K)$		
			a	bT	cT^{-2}
Rb_3UCl_6 (s)	-2272.103	447.16	232.128	0.06237448	458300
Rb_2UCl_5 (s)	-1803.391	354.95	184.012	0.05195632	458300
$RbUCl_4$ (s)	-1334.314	260.53	135.896	0.04153816	458300
Cs_3UCl_6 (s)	-2341.404	464.45	225.350	0.09740711	458300
Cs_2UCl_5 (s)	-1852.322	366.26	179.493	0.07531141	458300
$CsUCl_4$ (s)	-1361.955	270.08	133.637	0.05321570	458300
CsU_2Cl_7 (s)	-2231.835	430.98	221.417	0.08433570	916600

of the binary solution models were obtained from optimized models from the available databases and literature [6-9]. As optimized mixing energy parameters for the $RbCl$ - UCl_3 and $CsCl$ - UCl_3 binaries have not been reported, the mixing energies of these binaries could only be estimated to match the binary phase diagrams presented by F.D. Sutherland et al. [10]

Table 2. *Cation-cation coordination numbers used for MQM modeling of binary liquid solutions.*

A	B	Z^A_{AB}	Z^B_{AB}
Rb	U	2	6
Cs	U	3	6

$$\Delta g_{RbU/Cl} = -44750 + 2000\,\chi_{RbU} - 13800\chi_{URb}\ J\ mol^{-1} \quad (Eq.1)$$

$$\Delta g_{CsU/Cl} = -32650 - 19400\,\chi_{CsU} - 14000\chi_{UCs} - 2000\chi^2_{CsU} - 10000\chi^2_{UCs} - 205000\,\chi_{CsU}\chi_{UCs}\ Jmol^{-1} \quad (Eq.2)$$

Moreover, the solid solution mixing parameters for the UCl_3-$PuCl_3$ system were also revised to better match the experimental data reported by Morobei et al. [7].

$$\Delta G^{xs}_{ss,(U,Pu)Cl_3} = X_{UCl_3}X_{PuCl_3}\left[16250 - 4750\left(X_{UCl_3} - X_{PuCl_3}\right)\right] J\ mol^{-1} \quad (Eq.3)$$

A ternary interpolation was performed with $NaCl$, $MgCl_2$ and $(U,Pu)Cl_3$ as the end-members. In the optimized models, it can be noted that the $NaCl$-UCl_3, $NaCl$ - $PuCl_3$ and $NaCl$ - $MgCl_2$ interactions are described by negative mixing potentials, whereas the $MgCl_2$-UCl_3 and $MgCl_2$-$PuCl_3$ are characterized by positive mixing potentials. Hence, to augment the accuracy of this predictive model, the ternary interpolation was conducted using the Kohler interpolation technique along the $NaCl$-$MgCl_2$ and $NaCl$ - $(U,Pu)Cl_3$ axis, and the asymmetric Toop interpolation technique with $MgCl_2$ as the asymmetric component along the $MgCl_2$-$(U,Pu)Cl_3$ axes.

Subsequently, a pseudo-binary plot of the $NaCl$-$MgCl_2$ phase diagram was constructed by fixing the composition of $(U,Pu)Cl_3$ at the nominal value of 1.0 $mol\%$. The two compositions which demonstrated the lowest liquidus transition temperatures were selected as the optimum MSR fuel candidates. Using the FactSage 8.1 Equilibrium module, the effect of the target fission products $(RbCl, CsCl)$ on the candidate MSR fuel compositions was calculated through considerations of induced enthalpy change, liquidus temperature change, and the activities of intermediate compounds below liquidus temperature.

3. Results and Discussion

The $RbCl$ - UCl_3 and $CsCl$ - UCl_3 binary phase diagrams constructed using the MQM approximation are shown in Figure 1. It can be inferred that the fitted ΔG^{xs} parameters were able to reproduce the phase diagrams obtained from [10] with reasonable accuracy. To attest, most of the transition points from the original phase diagrams could be replicated to within relatively small margins of error: $\chi_{UCl_3} \pm 0.02$ and $T_{transition} \pm 10\ K$. The few anomalous points in our simulated phase diagrams which exceed the stipulated margins of error are summarized in Table 3.

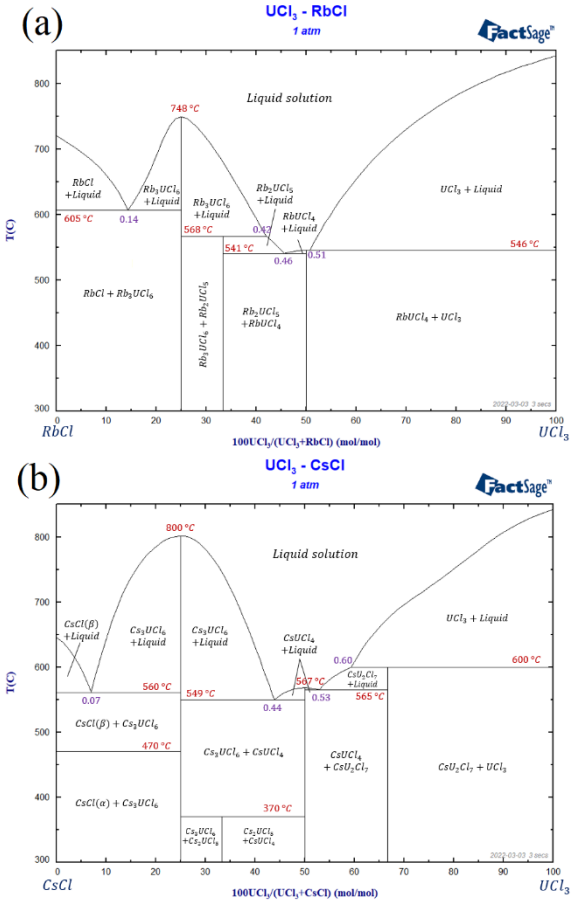

Figure 1. *Reconstructed binary phase diagrams of the (a) RbCl-UCl_3 and (b) CsCl-UCl_3 using the Modified Quasichemical Model on FactSage 8.1*

Since experimentally verified values for the thermodynamic data of intermediate compounds are not available, an alternative to evaluating the validity of our simulation parameters is to compare the mixing enthalpies with that of similar binaries. Figure 2(a) compares the mixing enthalpies of UCl_3 with other Group I chlorides, whereas Figure 2(b) compares the mixing enthalpies of our simulated binaries with two analogous systems: $RbCl$-$PuCl_3$ and $CsCl$-$PuCl_3$. It can be observed from Figure 2(a) that the magnitude

Table 3. *Anomalous points from simulated phase diagrams*

Phase Diagram	*Coordinates*	
	Simulated	*Reported*
$RbCl - UCl_3$	*Solidus* ($0.33 \leq \chi \leq 0.50, 541\ °C$)	*Solidus* ($0.33 \leq \chi \leq 0.50, 515\ °C$)
$CsCl - UCl_3$	*Eutectic point* $(0.07, 560°C)$ *Solidus* $(0.25 \leq \chi \leq 0.50, 549°C)$ *None*	*Eutectic point* $(0.12, 560°C)$ *Solidus* $(0.25 \leq \chi \leq 0.50, 530°C)$ *Peritectic* $(0.50 \leq \chi \leq 1.00, 550°C)$

of mixing enthalpies increases going down Group I. In addition, we can also observe that the optimized potential wells generally skew slightly to the left. In light of these trends, it becomes evident that the binaries modeled in this work match the descriptions very well. On the other hand, while the thermodynamic modeling of the KCl-UCl_3 system performed by Rose and Thomas [11] reproduces good binary phase diagrams, further analysis suggests that the mixing enthalpies derived from their modeling is excessively large (in magnitude) and deviates from the expected trends. However, comparisons with analogous binaries in Figure 2(b) indicate that the estimated potentials in this study may also be slightly more negative than the actual potentials. Experimentally verified thermochemical data of intermediate compounds in the estimated binaries would be needed to address this discrepancy.

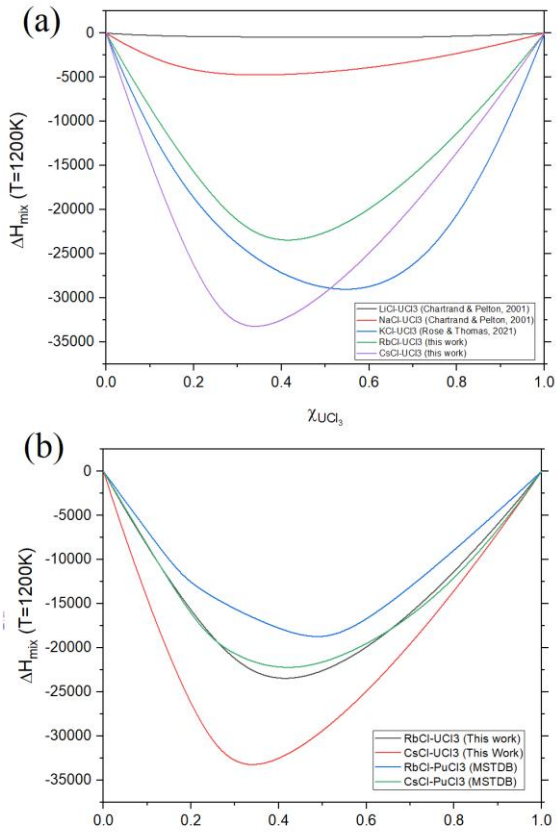

Figure 2. *(a) Comparison of mixing enthalpies between UCl_3 and other Group I chlorides at 1200 K. (b) Comparison of mixing enthalpies between $RbCl$-UCl_3, $CsCl$-UCl_3, $RbCl$-$PuCl_3$, $CsCl$-$PuCl_3$ at 1200 K.*

The activities of the end-members in the liquid state are another key parameter to assess the validity of MQM potentials used in thermodynamic modeling. Figure 3 depicts the calculated activities of the liquid-state end-member pairs in (a) $RbCl$-UCl_3 and $CsCl$-UCl_3 at 1200K. Assessment of other analogous binaries ($LiCl$-UCl_3 and $NaCl$-UCl_3) demonstrates a trend of decreasing activities near the intersection point between the activities of $M//Cl$ (M: *Group I element*) and $U//Cl$ going down the group. Moreover, the intersection points of these binaries are observed to be around χ_{UCl_3}~0.40 and

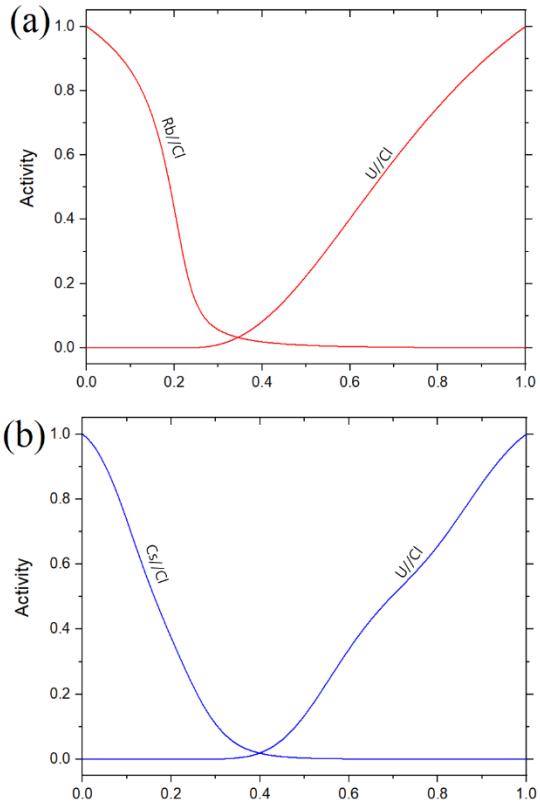

Figure 3. *Calculated activities of liquid end-member pairs in (a) $RbCl$-UCl_3 and $CsCl$-UCl_3 at 1200K.*

generally shift to the left going down the group. In that regard, it can be inferred that the calculated activities using our model matches the general trend of MCl-UCl_3 mixing, thereby further justifying the feasibility of our model.

The UCl_3-$PuCl_3$ binary phase diagram (Fig. 4) was also reconstructed after modifying the excess Gibbs' free energy for solid solution mixing (Eq.3). By modifying these parameters, we were able to reproduce the eutectic point $(0.74, 1002K)$ close to that reported by Morobei et al. $(0.74, 994K)$ [12].

Figure 5 displays the constructed ternary phase diagram with $NaCl$, $MgCl_2$, and $(U,Pu)Cl_3$ as the end-members. The calculated ternary phase diagram in this work is largely similar to that reported by Benes and Konings [6], except the smaller area occupied by the intermediate compounds $NaMgCl_3$ and Na_2MgCl_4. This is because the stoichiometry of the $(U,Pu)Cl_3$ used in this study was set to $U_{0.25}Pu_{0.75}Cl_3$ to reflect the eutectic composition of UCl_3-$PuCl_3$; while the composition used in their study is believed to be $U_{0.5}Pu_{0.5}Cl_3$. Hereinafter, the $U_{0.25}Pu_{0.75}Cl_3$ composition will be the only composition used in further calculations and will be referred to as *fissile content*.

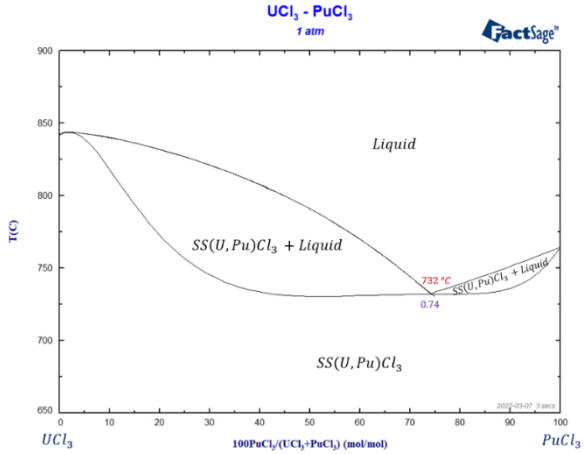

Figure 4. *Reconstructed* UCl_3 - $PuCl_3$ *binary phase diagram with modified solid solution mixing parameters*

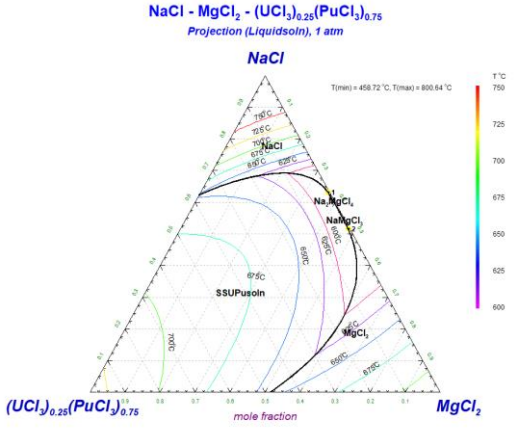

Figure 5. *Calculated liquidus surface projections of the* $NaCl$-$MgCl_2$-$U_{0.25}Pu_{0.75}Cl_3$ *system with isotherms at intervals of 25K.*

By fixing the fissile content at the nominal value of $1.0\,mol\%$, the pseudo-binary plot of the $NaCl$-$MgCl_2$ system (Fig.6) was constructed to help visualize the optimum fuel compositions that demonstrate the lowest liquidus transition temperatures. Two candidate compositions were derived (Table 5) and will henceforth be dubbed as *MSR*A* and *MSR*B*.

Table 4. *Phases present in the middle section of the pseudo-binary phase diagram (Fig.6)*

Region	Phases Present
A&B	$MgCl_2 + NaMgCl_3 + SS(U,Pu)\#1 + Liquid$
C	$NaMgCl_3 + SS(U,Pu)\#1 + SS(U,Pu)\#2 + Liquid$
D	$NaMgCl_3 + Na_2MgCl_4 + SS(U,Pu)\#1 + SS(U,Pu)\#2$
E	$NaMgCl_3 + SS(U,Pu)\#1 + Liquid$
F	$NaMgCl_3 + Na_2MgCl_4 + SS(U,Pu)\#1 + Liquid$
G	$Na_2MgCl_4 + SS(U,Pu)\#1 + Liquid$
H	$Na_2MgCl_4 + SS(U,Pu)\#1 + SS(U,Pu)\#2 + Liquid$
I	$NaCl + Na_2MgCl_4 + SS(U,Pu)\#1 + Liquid$

Table 5. *Chemical compositions of the two fuel candidates which demonstrate the lowest liquidus transition temperature*

Composition	χ_{NaCl}	χ_{MgCl_2}	$\chi_{U_{0.25}Pu_{0.75}Cl_3}$	T_{liq} (°C)
*MSR*A*	48.3	50.7	1.00	493
*MSR*B*	64.9	34.1	1.00	506

A simple model was adopted to account for the formation of the target fission isotope chlorides. In this model, it is assumed that the fissile isotopes undergo a simple fission process resulting in the formation of two species: (1) $RbCl\ or\ CsCl$ and (2) a corresponding species that is immiscible. The effective reaction can thus be described as follows:

$$U_{0.25}Pu_{0.75}Cl_3 \rightarrow (1-\alpha)\,U_{0.25}Pu_{0.75}Cl_3 + \alpha\,RbCl/CsCl \quad (Eq.4)$$

The isothermal change in enthalpy as a function of α at $600\,°C$ was plotted in Figure 7(a). It can be seen that the enthalpy was projected to increase linearly as a function of α for both *MSR*A* and *MSR*B*, with $RbCl$ having a slightly greater effect than $CsCl$. This is expected as the enthalpy of $RbCl$ is less negative compared to $CsCl$ at the stipulated temperature.

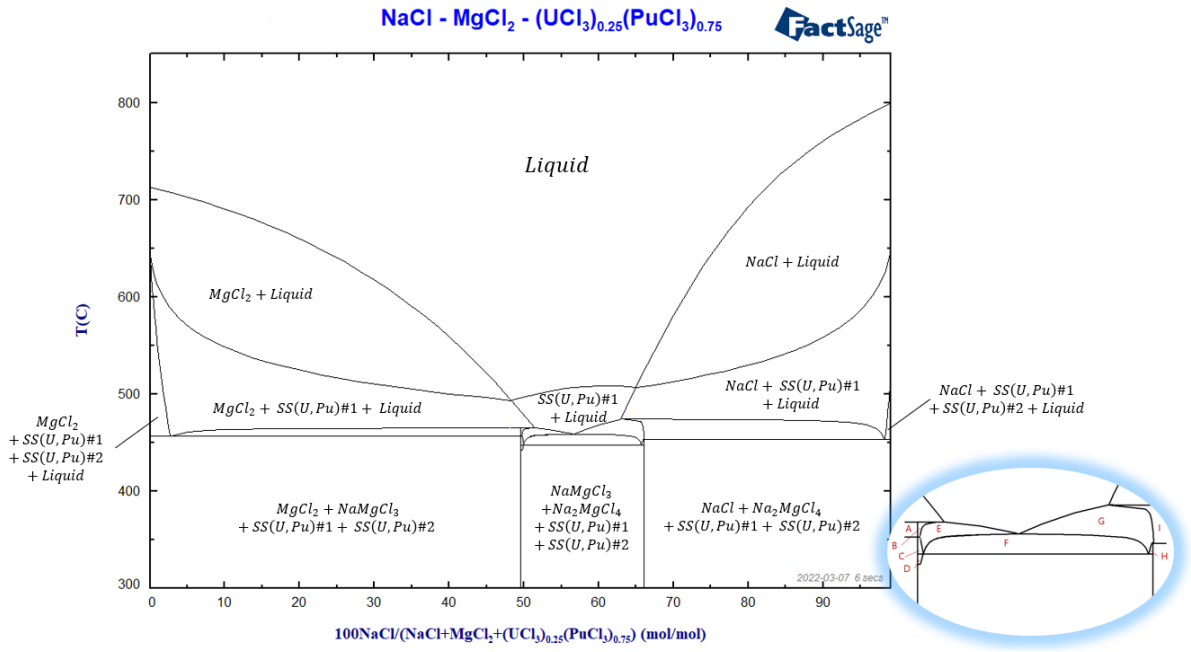

Figure 6. *Pseudo-binary* $\boldsymbol{NaCl\text{-}MgCl_2}$ *phase diagram plot assuming 1.0 mol%* $\boldsymbol{U_{0.25}Pu_{0.75}Cl_3}$

From the plots of liquidus transition temperature (T_{liq}) against fission isotope content in Figure 7(b), we observe opposing trends for *MSR*A* and *MSR*B*. T_{liq} decreases with fission isotope content for *MSR*A*; whereas T_{liq} increases with fission isotope content for *MSR*B*. A possible explanation for this discrepancy may be due to the difference in $NaCl$ content between the two compositions. In this context, pure $NaCl$ has a higher melting point compared to pure $MgCl_2$ and is known to form solid solutions with $RbCl$. It is proposed that a higher mole fraction of $NaCl$ in *MSR*B* provides more "free" $NaCl$ molecules to react with fission isotopes, hence leading to an overall increase in T_{liq}. However, considering the realistic concentrations of specific fission isotopes throughout the life cycle of normal MSR operation, it can be deduced that the induced change in T_{liq} due to fission isotopes is relatively small. Nonetheless, if all merits are to be taken into account, it becomes evident that *MSR*A* would be the more ideal fuel composition as lower melting temperatures for MSR fuel are typically associated with lower operating costs, higher heat transfer efficiency, and larger margins of safety.

To probe the effect of fission products on the fuel chemistry, the activities of several representative intermediate compounds were plotted as functions of χ_{NaCl} in Figures 8(a) and (b). The concentration of fission product species was set at 0.1 mol%. It was found that the activities of the intermediate compounds were the highest at both ends of the

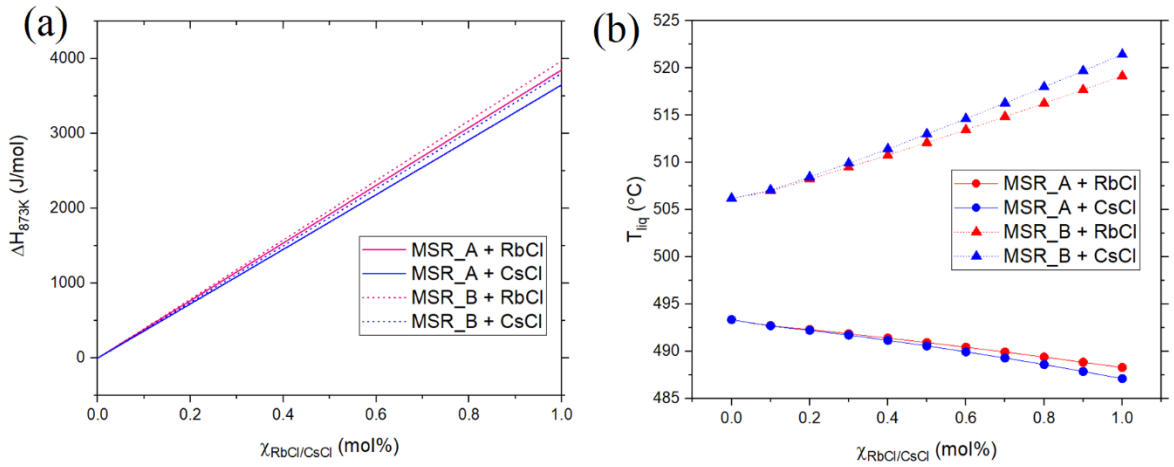

Figure 7 *(a) Calculated enthalpy change of MSR Fuel w.r.t fission isotope content at* $\boldsymbol{600\ °C}$*; (b) Calculated change in liquidus transition temperature w.r.t fission isotope content.*

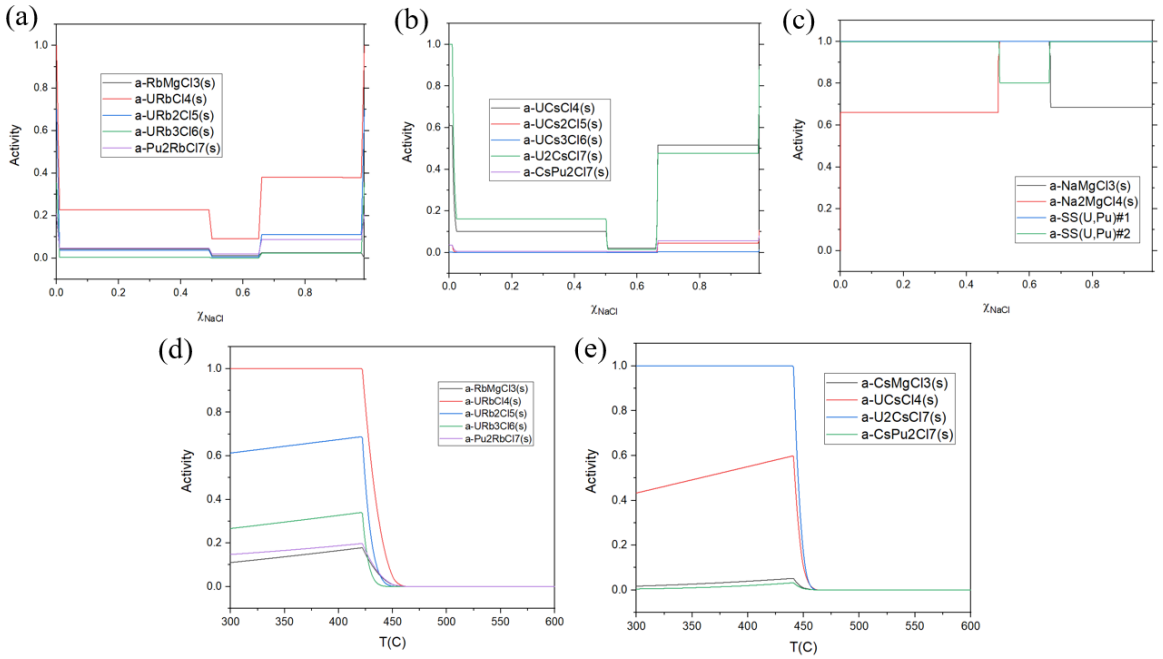

Figure 8. *Activities of various intermediate compounds in MSR*A with (a)* $\mathbf{0.1\ mol\%\ RbCl\ at\ 440\ °C}$, *(b)* $\mathbf{0.1\ mol\%\ CsCl\ at\ 450°C}$, *(c)* $\mathbf{no\ fission\ isotopes\ at\ 450°C}$ *w.r.t to NaCl content, (d)* $\mathbf{0.1\ mol\%\ RbCl}$ *and (e)* $\mathbf{0.1\ mol\%\ CsCl}$ *w.r.t temperature.*

spectrum. One possible explanation may be attributed to the configurational entropy for solution mixing being exponentially larger in the middle of the spectrum. Consequently, fission products can be uniformly distributed within the mixture and the formation of stoichiometric intermediate compounds is rendered essentially negligible. In contrast, the number of mixing configurations becomes considerably smaller at the ends of the spectrum. In this case, the effective concentration of the less dominant species becomes comparable to that of the fission isotopes and can thus "actively" react to form stoichiometric intermediate compounds, therefore accounting for the increased activities of intermediate compounds at the opposite ends of the spectrum.

Another interesting feature that can be inferred from Figures 8(a) and (b) is the "valley" in the region $0.500 < \chi_{NaCl} < 0.667$, whereby the activities of all intermediate compounds correspond to a minimum. Captivatingly, this region corresponds exactly to the region whereby the activities of $NaMgCl_3$, Na_2MgCl_4, and both solid solutions of $(U,Pu)Cl_3$ plateau at the absolute maximum (Figure 8(c)). This further corroborates our previous explanation that the consumption of all the available cations in the middle of the spectrum, to form more dominant stoichiometric intermediate compounds, limits the formation of intermediate compounds with the fission isotopes species.

Figures 8(c) and (d) project the activities of various intermediate compounds in the *MSR*A* composition with respect to temperature. A precipitous decline in the activities of all the intermediate compounds can be observed inside the temperature range $420\text{-}470°C$. Given the normal MSR operating conditions $T \geq 600\ °C$, we can infer that the introduction of Group I fission isotopes Rb and Cs does not bear any significant effects on the fuel chemistry of *MSR*A*—and in extension, the spectrum of compositions between *MSR*A* and *MSR*B*.

4. Conclusions

In this work, we reconstructed 14 binary phase diagrams between combinations of the chloride salts: $NaCl, MgCl_2, UCl_3, PuCl_3, RbCl, and\ CsCl$, using the Modified Quasichemical Model (MQM). While the parameters used in the modeling of the $RbCl\text{-}UCl_3$ and $CsCl\text{-}UCl_3$ binaries were estimated, the remaining phase diagrams were all constructed using optimized parameters. The validity of our estimates was assessed through comparisons of the calculated solution mixing enthalpies and activities of liquid species with that of analogous binary systems. While our estimated binaries agree well with the general trend of $MCl\text{-}AnCl_3$ $(M: Group\ I, An: Actinide)$ binary mixtures, the magnitude of the mixing potentials are adjudged to be slightly large. Experimentally verified data is needed to optimize the mixing parameters.

The results above were then used to model the effects of Group I fission products (Cs, Rb) on the phase behavior of the candidate MSR fuel $NaCl\text{-}$

$MgCl_2$-UCl_3-$PuCl_3$. Given the fixed fissile content of 1.0 mol% $U_{0.25}Pu_{0.75}Cl_3$, we projected no significant alteration to the fuel chemistry under normal operating conditions. In fact, we found that the intermediate compounds induced by fission isotopes only form at relatively low temperatures and primarily on opposite ends of the $NaCl$-$MgCl_2$ spectrum. We believe that this work provides new insight into the modeling of the effect of fission isotopes on the performance of MSR fuels.

5. Acknowledgments

This study is supported by the research project funded by The Circle Foundation.

6. References

[1] Locatelli, G., Mancini, M., & Todeschini, N. (2013). Generation IV nuclear reactors: Current status and future prospects. Energy Policy, 61, 1503–1520. https://doi.org/10.1016/j.enpol.2013.06.101

[2] Betzler, B. R., Heidet, F., Feng, B., Rabiti, C., Sofu, T., & Brown, N. R. (2019). Modeling and simulation functional needs for molten salt reactor licensing. Nuclear Engineering and Design, 355(August), 110308. https://doi.org/10.1016/j.nucengdes.2019.110308

[3] Beneš, O., & Souček, P. (2020). Molten salt reactor fuels. Advances in Nuclear Fuel Chemistry, 249–271. https://doi.org/10.1016/b978-0-08-102571-0.00007-0

[4] Ocádiz Flores, J. A., Konings, R. J. M., & Smith, A. L. (2022). Using the Quasi-chemical formalism beyond the phase Diagram: Density and viscosity models for molten salt fuel systems. Journal of Nuclear Materials, 561, 153536. https://doi.org/10.1016/j.jnucmat.2022.153536

[5] Wang, Z. B., Hu, H. X., & Zheng, Y. G. (2018). Synergistic effects of fluoride and chloride on general corrosion behavior of AISI 316 stainless steel and pure titanium in H2SO4 solutions. Corrosion Science, 130(October 2017), 203–217. https://doi.org/10.1016/j.corsci.2017.10.028

[6] Beneš, O., & Konings, R. J. M. (2008). Thermodynamic evaluation of the NaCl-MgCl2-UCl3-PuCl3 system. Journal of Nuclear Materials, 375(2), 202–208. https://doi.org/10.1016/j.jnucmat.2008.01.007

[7] Oak Ridge National Laboratory, Molten Salt Thermodynamic Database, MSTDB (n.d.), https://code.ornl.gov/neams/mstdb, (Accessed 15 January, 2022)

[8] Agca, C., Johnson, K., Mcmurray, J., Yingling, J., & Besmann, T. (2021). FY21 status report on the Molten Salt Thermal Properties Database (MSTDB) development. 20. https://www.osti.gov/servlets/purl/1814280/%0Ahttps://info.ornl.gov/sites/publications/Files/Pub161288.pdf

[9] Chartrand, P., & Pelton, A. D. (2001). Thermodynamic evaluation and optimization of the LiCl-NaCl-KCl-RbCl-CsCl-MgCl2-CaCl2 system using the modified quasi-chemical model. Metallurgical and Materials Transactions A: Physical Metallurgy and Materials Science, 32(6), 1361–1383. https://doi.org/10.1007/s11661-001-0227-2

[10] Sutherland Phase Diagram - Argonne National Laboratory. (n.d.). Retrieved March 9, 2022, from https://www.ne.anl.gov/nce/pyroprocess-conference/presentations/Wednesday_PM/Sutherland_Phase%20Diagram.pdf

[11] Rose, M., & Thomas, S. (2021). Production and Chemical Analysis of NaCl-KCl-UCl3 Salts. https://www.osti.gov/biblio/1773495%0Ahttps://www.osti.gov/servlets/purl/1773495%0Ahttps://www.osti.gov/servlets/purl/1773495/

[12] M.P. Morobei, V.N. Desyatnik, O.V. Skiba, N.M. Emel'yanov, Russ. J. Inorg. Chem. 18 (1973) 1628.